Dynamical density functional theory for anisotropic colloidal particles

M. Rex, H. H. Wensink, and H. Löwen
Institut für Theoretische Physik II: Weiche Materie, Heinrich-Heine-Universität Düsseldorf, Universitätsstraße 1, 40225 Düsseldorf, Germany

(Received 14 June 2007; published 24 August 2007)

We generalize the formalism of dynamical density functional theory for translational Brownian dynamics toward that of anisotropic colloidal particles which perform both translational and rotational Brownian motion. Using a mean-field approximation for the density functional and a Gaussian-segment model for the rod interaction, the dynamical density functional theory is then applied to a concentrated rod suspension in a confined slab geometry made by two parallel soft walls. The walls are either expanded or compressed and the relaxation behavior is investigated for an equilibrated starting configuration. We find distinctly different orientational ordering during expansion and compression. During expansion we observe preferential parallel ordering of the rods relative to the wall while during compression there is homeotropic ordering perpendicular to the wall. We find a nonexponential relaxation behavior in time. Furthermore, an external field which aligns the rods perpendicular to the walls is turned on or switched off and similar differences in the relaxational dynamics are found. Comparing the theoretical predictions to Brownian dynamics computer simulation data, we find good agreement.

DOI: 10.1103/PhysRevE.76.021403 PACS number(s): 82.70.Dd, 64.70.Md, 61.20.Gy, 61.30.Pq

I. INTRODUCTION

Classical density functional theory (DFT) is a microscopic theory which starts from the interparticle interactions and bulk fluid correlations as an input and predicts the inhomogeneous density profiles in an external potential including strongly inhomogeneous situations like freezing; for reviews, see [1,2]. The results are in quantitative agreement with simulation data and different approximations for the density functional are available for various interparticle interactions. For example, Rosenfeld's fundamental measure theory [3,4] has been shown to be reliable for hard spheres and the mean-field approximation is asymptotically correct for soft core interaction at high densities [5–7].

While it is by now well-understood how to extract the static equilibrium properties of an inhomogeneous system from density functional theory, its extension toward time-dependent dynamical situations in nonequilibrium is more challenging. Recently, a dynamical density functional theory (DDFT) was developed [8–10] for Brownian dynamics which is the appropriate dynamics for colloidal suspensions. DDFT results for the nonequilibrium dynamics of inhomogeneous Brownian fluids were found to agree with simulation data [11–13]. Further important activities in developing the dynamical extension of DFT lie in the existence proof of the dynamical functional [14], its ability to be applicable for Newtonian dynamics [15], and to include fluctuations and noise effects [16].

All activities in dynamical density functional theory were focused on translational dynamics while the orientational degrees of freedom were neglected. The latter are trivial for spherical particles but become highly relevant for asymmetric (e.g., rodlike) particles. At high densities, the translational degrees of freedom are nontrivially coupled to their rotational counterparts.

In this paper, we extend the formalism of dynamical density functional theory to both translational and rotational degrees of motion by considering the Brownian motion of anisotropic colloidal particles. With similar approximations used for the translational case [10], we derive the dynamical equation for the time-dependent density field $\rho(\mathbf{r},\hat{\omega},t)$ which depends both on the position $\mathbf{r}$ and orientation $\hat{\omega}$, where $\hat{\omega}$ is a unit vector. It is shown that this theory becomes equivalent to the approach of Dhont, Briels, and co-workers [17,18] at low density, where a virial approximation for the density functional is appropriate. The theory, however, provides a more general framework for dynamics and nonequilibrium phenomena at higher densities as well. We then test the theory against Brownian dynamics computer simulation for a soft-core rod-segment model. This model is the rodlike analog to spherical polymer models [19,20] and therefore describes bottlebrush polymers with a stiff backbone [21–23]. We use a mean-field-type approximation for the density functional and apply it to a situation of strong confinement between two soft walls. Two situations are studied. First the confined system is compressed and relaxed by compressing and expanding the walls. In a second setup, an additional external aligning field is turned on and switched off. We find a nontrivial relaxation behavior which is nonexponential in time. Expansion and compression proceed via different paths as a function of time. In particular, distinctly different orientational ordering during expansion and compression is observed. During expansion, rods orient preferentially parallel to the wall while during compression there is homeotropic ordering perpendicular to the wall. Similar conclusions are found for the aligning field. In general, good agreement between DDFT and Brownian dynamics simulation is found.

The paper is organized as follows. In Sec. II, we derive the generalized dynamical density functional theory which includes rotational Brownian motion. Sections III and IV will be devoted to describing the rod model, the associated free energy functional, and the dynamical processes, respectively. In Sec. V, the predictions of our DDFT will be compared with simulation results and notable effects will be dis-

cussed. Finally, some conclusions will be formulated in Sec. VI.

II. EQUATION OF MOTION FOR THE ONE-BODY DENSITY

In this section, we will derive an expression for the time evolution of the one-body density, $\rho(\mathbf{r},\hat{\omega},t)$, for anisotropic Brownian particles with a three-dimensional spatial coordinate $\mathbf{r}$ and orientation unit vector $\hat{\omega}$. In doing so, we generalize the derivation by Archer and Evans [10] to orientational degrees of freedom.

We start from the full probability density distribution $P(\mathbf{r}^N,\hat{\omega}^N,t)$ to find N anisotropic Brownian particles at positions $\mathbf{r}^N=(\mathbf{r}_1,\ldots,\mathbf{r}_N)$ and orientations $\hat{\omega}^N=(\hat{\omega}_1,\ldots,\hat{\omega}_N)$. According to Ref. [10], the n-body density is given by the following integral of the probability density distribution $P(\mathbf{r}^N,\hat{\omega}^N,t)$:

$$\rho^n(\mathbf{r}^n,\hat{\omega}^n,t)=\frac{N!}{(N-n)!}\int d\mathbf{r}_{n+1}\ldots\int d\mathbf{r}_N\oint d\hat{\omega}_{n+1}\ldots\oint d\hat{\omega}_N \times P(\mathbf{r}^N,\hat{\omega}^N,t), \tag{1}$$

where the integral of the orientation is over the full unit sphere. For overdamped Brownian dynamics of the particles, the time evolution of $P(\mathbf{r}^N,\hat{\omega}^N,t)$ is given by the Smoluchowski equation [24].

$$\frac{\partial P(\mathbf{r}^N,\hat{\omega}^N,t)}{\partial t}=\hat{\mathcal{L}}_S P(\mathbf{r}^N,\hat{\omega}^N,t), \tag{2}$$

where the Smoluchowski operator is defined as

$$\hat{\mathcal{L}}_S=\sum_{i=1}^{N}\{\nabla_{\mathbf{r}_i}\cdot\mathbf{D}(\hat{\omega}_i)\cdot[\nabla_{\mathbf{r}_i}+\beta\nabla_{\mathbf{r}_i}U(\mathbf{r}^N,\hat{\omega}^N,t)] + D_r\hat{\mathcal{R}}_i\cdot[\hat{\mathcal{R}}_i+\beta\hat{\mathcal{R}}_i U(\mathbf{r}^N,\hat{\omega}^N,t)]\}. \tag{3}$$

Here, hydrodynamic interactions are not taken into account, $\beta^{-1}=k_BT$ is the thermal energy of the system, $\nabla_{\mathbf{r}_i}$ is the gradient operator with respect to $\mathbf{r}_i$, and $\hat{\mathcal{R}}_i$ is the rotation operator acting on the Cartesian coordinates of the orientation $\hat{\omega}_i$. The latter is given by

$$\hat{\mathcal{R}}_i=\hat{\omega}_i\times\nabla_{\hat{\omega}_i}. \tag{4}$$

Furthermore, D_r is the rotational diffusion coefficient and $\mathbf{D}(\hat{\omega}_\mathbf{i})$ the translational diffusion tensor. For uniaxial (cylindrical) anisotropic particles this tensor may be expressed as

$$\mathbf{D}(\hat{\omega}_i)=D_\parallel\hat{\omega}_i\hat{\omega}_i+D_\perp[\hat{\mathbf{I}}-\hat{\omega}_i\hat{\omega}_i], \tag{5}$$

in terms of the translational diffusion constant parallel ($D_\parallel$) and perpendicular ($D_\perp$) to the main particle axis $\hat{\omega}_i$, with $\hat{\mathbf{I}}$ the unit matrix and $\hat{\omega}_i\hat{\omega}_i$ the dyadic product. Assuming pairwise additivity for the total potential energy of the system $U(\mathbf{r}^N,\hat{\omega}^N,t)$, we may write

$$U(\mathbf{r}^N,t)=\sum_{i=1}^{N}V_{\text{ext}}(\mathbf{r}_i,\hat{\omega}_i,t)+\frac{1}{2}\sum_{j\neq i}^{N}\sum_{i=1}^{N}v_2(\mathbf{r}_i,\mathbf{r}_j,\hat{\omega}_i,\hat{\omega}_j), \tag{6}$$

where $V_{\text{ext}}(\mathbf{r},\hat{\omega},t)$ is the one-body external potential acting on each particle and $v_2(\mathbf{r},\mathbf{r}',\hat{\omega},\hat{\omega}')$ is the pair potential. Upon integrating Eq. (2) with $N\int d\mathbf{r}_2\ldots\int d\mathbf{r}_N\oint d\hat{\omega}_2\ldots\oint d\hat{\omega}_N$, one obtains

$$\frac{\partial\rho(\mathbf{r},\hat{\omega},t)}{\partial t}=\nabla_\mathbf{r}\cdot\mathbf{D}(\hat{\omega})\cdot[\nabla_\mathbf{r}\rho(\mathbf{r},\hat{\omega},t) + \beta\rho(\mathbf{r},\hat{\omega},t)\nabla_\mathbf{r}V_{\text{ext}}(\mathbf{r},\hat{\omega},t)-\beta\overline{\mathbf{F}}(\mathbf{r},\hat{\omega},t)] + D_r\hat{\mathcal{R}}\cdot[\hat{\mathcal{R}}\rho(\mathbf{r},\hat{\omega},t)+\beta\rho(\mathbf{r},\hat{\omega},t)\hat{\mathcal{R}}V_{\text{ext}}(\mathbf{r},\hat{\omega},t) - \beta\overline{\mathbf{T}}(\mathbf{r},\hat{\omega},t)], \tag{7}$$

with $\overline{\mathbf{F}}(\mathbf{r},\hat{\omega},t)$ denoting the average force and $\overline{\mathbf{T}}(\mathbf{r},\hat{\omega},t)$ the average torque due to the interaction with other particles:

$$\overline{\mathbf{F}}(\mathbf{r},\hat{\omega},t)=-\int d\mathbf{r}'\oint d\hat{\omega}'\rho^{(2)}(\mathbf{r},\mathbf{r}',\hat{\omega},\hat{\omega}',t)\nabla_\mathbf{r}v_2(\mathbf{r},\mathbf{r}',\hat{\omega},\hat{\omega}',t)$$

and

$$\overline{\mathbf{T}}(\mathbf{r},\hat{\omega},t)=-\int d\mathbf{r}'\oint d\hat{\omega}'\rho^{(2)}(\mathbf{r},\mathbf{r}',\hat{\omega},\hat{\omega}',t)\hat{\mathcal{R}}v_2(\mathbf{r},\mathbf{r}',\hat{\omega},\hat{\omega}',t). \tag{8}$$

Note that for the steady-state ($\partial\rho/\partial t=0$), Eq. (7) reduces to the first member of the Yvon-Born-Green (YBG) hierarchy for molecular fluids [25].

The equation of motion (7) for the one-body density $\rho(\mathbf{r},\hat{\omega},t)$ is *exact* but depends on the unknown time-dependent two-body density $\rho^{(2)}(\mathbf{r},\mathbf{r}',\hat{\omega},\hat{\omega}',t)$. Using Eq. (1), a similar equation of motion may be derived for $\rho^{(2)}(\mathbf{r},\mathbf{r}',\hat{\omega},\hat{\omega}',t)$ which will depend on the three-body density $\rho^{(3)}$ and so on. To make headway, a closure relation is needed to terminate the resulting hierarchy of coupled equations of motion. As in static DFT, this can be done at the second YBG level by recasting the average interaction force and torque, given by Eq. (8), into functionals of the nonequilibrium one-body density to construct a dynamical density functional theory.

In equilibrium, a generalized force balance equation can be proved [26,27]

$$\nabla_\mathbf{r}\rho_0(\mathbf{r},\hat{\omega})+\beta\rho_0(\mathbf{r},\hat{\omega})\nabla_\mathbf{r}V_{\text{ext}}(\mathbf{r},\hat{\omega}) = -\rho_0(\mathbf{r},\hat{\omega})\nabla_\mathbf{r}\left.\frac{\delta\mathcal{F}_{\text{exc}}[\rho]}{\delta\rho}\right|_{\rho=\rho_0(\mathbf{r},\hat{\omega})}, \tag{9}$$

where $\rho_0(\mathbf{r},\hat{\omega})$ denotes the equilibrium one-particle density field corresponding to the prescribed external potential $V_{\text{ext}}(\mathbf{r},\hat{\omega})$ and $\mathcal{F}_{\text{exc}}[\rho_0]$ is the excess free energy density functional in equilibrium. Likewise, a generalized torqued balance [27] reads in equilibrium as

$$\hat{\mathcal{R}}\rho_0(\mathbf{r},\hat{\omega}) + \beta\rho_0(\mathbf{r},\hat{\omega})\hat{\mathcal{R}}V_{\text{ext}}(\mathbf{r},\hat{\omega}) = -\rho_0(\mathbf{r},\hat{\omega})\hat{\mathcal{R}}\left.\frac{\delta\mathcal{F}_{\text{exc}}[\rho]}{\delta\rho}\right|_{\rho=\rho_0(\mathbf{r},\hat{\omega})}. \tag{10}$$

A second set of balance conditions are the well-known YBG relations [cf. Eq. (7)] in equilibrium [25]. These are for the translational part

$$\nabla_{\mathbf{r}}\rho_0(\mathbf{r},\hat{\omega}) + \beta\rho_0(\mathbf{r},\hat{\omega})\nabla_{\mathbf{r}}V_{\text{ext}}(\mathbf{r},\hat{\omega}) = -\beta\int d\mathbf{r}'\oint d\hat{\omega}'\rho_0^{(2)}(\mathbf{r},\mathbf{r}',\hat{\omega},\hat{\omega}')\nabla_{\mathbf{r}}v_2(\mathbf{r},\mathbf{r}',\hat{\omega},\hat{\omega}') \tag{11}$$

and for the rotational part

$$\hat{\mathcal{R}}\rho_0(\mathbf{r},\hat{\omega}) + \beta\rho_0(\mathbf{r},\hat{\omega})\hat{\mathcal{R}}V_{\text{ext}}(\mathbf{r},\hat{\omega}) = -\beta\int d\mathbf{r}'\oint d\hat{\omega}'\rho_0^{(2)}(\mathbf{r},\mathbf{r}',\hat{\omega},\hat{\omega}')\hat{\mathcal{R}}v_2(\mathbf{r},\mathbf{r}',\hat{\omega},\hat{\omega}'), \tag{12}$$

respectively. Consequently, the following two relations hold in equilibrium:

$$\rho_0(\mathbf{r},\hat{\omega})\nabla_{\mathbf{r}}\frac{\delta\mathcal{F}_{\text{exc}}[\rho]}{\delta\rho_0(\mathbf{r},\hat{\omega})} = \int d\mathbf{r}'\oint d\hat{\omega}'\rho_0^{(2)}(\mathbf{r},\mathbf{r}',\hat{\omega},\hat{\omega}')\nabla_{\mathbf{r}}v_2(\mathbf{r},\mathbf{r}',\hat{\omega},\hat{\omega}') \tag{13}$$

and

$$\rho_0(\mathbf{r},\hat{\omega})\hat{\mathcal{R}}\frac{\delta\mathcal{F}_{\text{exc}}[\rho]}{\delta\rho_0(\mathbf{r},\hat{\omega})} = \int d\mathbf{r}'\oint d\hat{\omega}'\rho_0^{(2)}(\mathbf{r},\mathbf{r}',\hat{\omega},\hat{\omega}')\hat{\mathcal{R}}v_2(\mathbf{r},\mathbf{r}',\hat{\omega},\hat{\omega}'). \tag{14}$$

The two right-hand sides of Eqs. (13) and (14) occur in the dynamical (nonequilibrium) context as average force and torque in Eq. (7). The basic approximation now is to use this expression in the nonequilibrium situation. This may be called an adiabatic approximation since the underlying idea is to identify—for a fixed time t—the dynamical one-particle density profile $\rho(\mathbf{r},\hat{\omega},t)$ with an equilibrium density profile $\rho_0(\mathbf{r},\hat{\omega})$ with a suitably prescribed external potential. Strictly speaking, the two latter quantities depend parametrically on time t. Hence nonequilibrium correlations are approximated by equilibrium correlations of a suitable equilibrium reference system that possesses the same one-particle density [8,9].

Within this *adiabatic approximation*, we obtain our central dynamical density functional theory (DDFT) result:

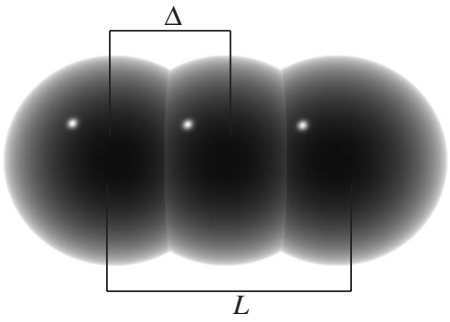

FIG. 1. Gaussian segment model of $N_S=3$ and segment spacing Δ.

$$\frac{\partial\rho(\mathbf{r},\hat{\omega},t)}{\partial t} = \nabla_{\mathbf{r}}\cdot\mathbf{D}(\hat{\omega})\cdot\left[\rho(\mathbf{r},\hat{\omega},t)\nabla_{\mathbf{r}}\frac{\delta\mathcal{F}[\rho(\mathbf{r},\hat{\omega},t)]}{\delta\rho(\mathbf{r},\hat{\omega},t)}\right] + D_r\hat{\mathcal{R}}\cdot\left[\rho(\mathbf{r},\hat{\omega},t)\hat{\mathcal{R}}\frac{\delta\mathcal{F}[\rho(\mathbf{r},\hat{\omega},t)]}{\delta\rho(\mathbf{r},\hat{\omega},t)}\right], \tag{15}$$

in terms of the total *equilibrium* Helmholtz free energy functional

$$\mathcal{F}[\rho_0] = \mathcal{F}_{\text{id}}[\rho_0] + \mathcal{F}_{\text{exc}}[\rho_0] + \int d\mathbf{r}\oint d\hat{\omega}\,\rho_0(\mathbf{r},\hat{\omega})V_{\text{ext}}(\mathbf{r},\hat{\omega},t), \tag{16}$$

where the ideal contribution reads

$$\mathcal{F}_{\text{id}}[\rho_0] = k_{\text{B}}T\int d\mathbf{r}\oint d\hat{\omega}\,\rho_0(\mathbf{r},\hat{\omega})[\ln\mathcal{V}\rho_0(\mathbf{r},\hat{\omega}) - 1], \tag{17}$$

with $\mathcal{V}$ the thermal volume of the anisotropic particle.

We finish this section with some remarks: First of all, the DDFT equation for spherical particles is recovered when the density is independent of orientation. In this case, the adiabatic approximation has been shown to hold even for strong inhomogeneities and strong time dependencies and turned out to give remarkably good agreement with results from Brownian dynamics computer simulations [7,10–13,16,28–31]. Second, we emphasize that the above equation reproduces the approach proposed by Dhont and Briels [17,18] for thin hard rods if $\mathcal{F}_{\text{exc}}[\rho_0]$ is represented by the Onsager functional [32,33]. Third, a similar dynamical density functional theory approach was proposed by Chandra and Bagchi [34,35] on a phenomenological basis. In the latter work, the explicit coupling between orientational and translational diffusion was neglected.

III. MODEL AND FREE ENERGY FUNCTIONAL

In this work, we consider systems of soft rods of length L, each composed of N_S segments of *ultrasoft* spheres; see Fig. 1 [65]. The distance between two consecutive segments on the rod is $\Delta=L/(N_S-1)$. The interaction potential between two segments of different rods is supposed to be a Gaussian. The total rod-rod interaction potential is then given by

$$v_2(\mathbf{r}_i,\mathbf{r}_j,\hat{\omega}_i,\hat{\omega}_j) = \epsilon \sum_{\alpha=-K}^{K} \sum_{\beta=-K}^{K} \exp\left(-\frac{|\mathbf{r}_{\alpha\beta}|^2}{\sigma^2}\right), \tag{18}$$

where $K=(N_S-1)/2$ and $\mathbf{r}_{\alpha\beta}=(\mathbf{r}_i+\alpha\Delta\hat{\omega}_i)-(\mathbf{r}_j+\beta\Delta\hat{\omega}_j)$ is the distance between segment α on rod i and β on rod j $(i\neq j)$. Furthermore, σ is the range of the Gaussian potential which sets the unit length and $\epsilon=k_BT$ provides the unit of energy for the system. In all cases, we consider slightly anisotropic rods with $N_S=3$ and $L\equiv\sigma$.

The Gaussian segment model can be considered as a simplified model for the effective interaction between so-called *bottlebrush* polymers with a short, stiff backbone [21–23]. For ultrasoft particles at high densities, a very accurate and simple functional $\mathcal{F}_{\text{exc}}[\rho]$ is available, namely the *mean-field* or *random-phase* approximation:

$$\mathcal{F}_{\text{exc}}[\rho] = \frac{1}{2}\int d\mathbf{r}\int d\mathbf{r}'\oint d\hat{\omega}\oint d\hat{\omega}'\,\rho(\mathbf{r},\hat{\omega})v_2(\mathbf{r},\mathbf{r}',\hat{\omega},\hat{\omega}') \times\rho(\mathbf{r}',\hat{\omega}'), \tag{19}$$

which was demonstrated to become exact for bounded potentials at asymptotically high densities [5–7]. The accuracy of the static mean-field DFT for soft rods enables us to scrutinize the validity of the adiabatic approximation for the dynamics of systems with coupled translational and rotational degrees of freedom.

An important limitation of our model is that, within the mean-field approximation, the rotational diffusion becomes ideal for homogeneous systems. This can be easily inferred from the excess functional Eq. (19) using the rod pair potential Eq. (18). Identifying $\rho(\mathbf{r},\hat{\omega})=\rho$ and carrying out the spatial integration over the Gaussian potential leads to a constant, independent of the orientation. This result, which in fact holds for *any* bounded segment-segment potential, implies that in homogeneous systems all rotational correlations are absent and that the system cannot form a stable nematic phase. Although this effect may seem unphysical, it is in fact reproduced by Brownian dynamics simulations of the segment model provided that the density is sufficiently high [36]. Therefore, in order to avoid the rotational diffusion being trivial we will only consider inhomogeneous systems throughout this paper. This is done by confining the fluid in a slab geometry consisting of two soft walls, see Fig. 2, so that a nonuniform density distribution is generated. The soft walls are supposed to model an optical trap such that only the colloidal particles are affected by the field and the solvent remains quiescent. For the external wall potential, we choose the following form:

$$V_{\text{wall}}(z,t) = V_0[z/Z(t)]^{10}. \tag{20}$$

Here, $V_0=10k_BT$ is the amplitude of the potential and $Z(t)$ the potential range that will be changed in time; see Sec. IV. In this setup, the instantaneous density profile $\rho(z,\vartheta,t)$ depends on only one spatial coordinate z (normal to the wall), an angular one ϑ (the angle between the rod and the wall normal), and time t. A similar setup for the statics of hard ellipsoids between hard walls was studied by Chrzanowska *et al.* [37].

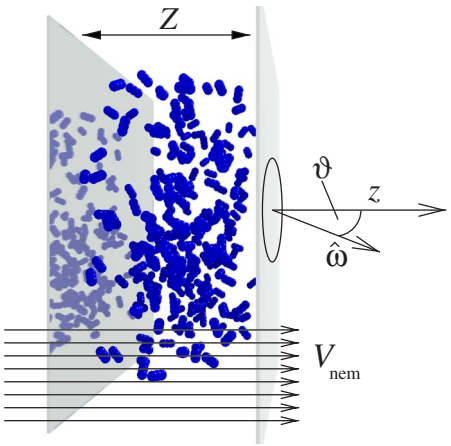

FIG. 2. (Color online) Schematic sketch of the system setup. The Gaussian rods are confined in a slab geometry that consists of two soft walls and an orienting field. V_{nem} is applied perpendicular to the walls. The relevant coordinates of the system are the spatial coordinate z normal to the wall and the angle ϑ between the rod and the wall normal.

IV. DYNAMIC PROCESSES

We intend to study two different setups. First, the system is compressed and expanded by changing the wall separation $Z(t)$. For the compression case, the wall separation is reduced linearly in time, so that

$$Z(t) = \begin{cases} 2\sigma & \text{if } t<0, \\ 2\sigma - ct & \text{if } 0\le t\le \tau_B, \\ \sigma & \text{if } t>\tau_B, \end{cases} \tag{21}$$

with the velocity of the wall $c=\sigma/\tau_B$. τ_B denotes the Brownian time scale and will be specified later. The reverse direction is implemented for the expansion case. Additionally, we investigate the expansion process for an instantaneous extension of the wall separation. We do not look at the inverse problem: The instantaneous compression.

In a second setup, we instantaneously switch on an external orienting field represented by

$$V_{\text{nem}}(\vartheta) = -\Phi_0\cos^2\vartheta, \tag{22}$$

where the strength of the potential is $\Phi_0=10k_BT$ and ϑ is the angle between the wall normal and the orientation of the rods: $\cos\vartheta=\hat{z}\cdot\hat{\omega}$. This field generates strong homeotropic nematic ordering with a director parallel to the wall normal. All setups are summarized in Table I.

In each system the initial density is the equilibrium density $\rho_0(z,\vartheta,t_0)$ of the respective system and we follow the

TABLE I. All setups investigated in this manuscript which are characterized by different time-dependent external potentials and labeled by the letters A–E. In A, B, and C a slab confinement of two soft walls is modeled with time varying wall separation $Z(t)$ *compressing or relaxing the system.* z is the coordinate perpendicular to the walls, $V_0=10k_BT$, and $c=\sigma/\tau_B$. In D and E, in addition to a fixed slab geometry, a nematic ordering field is either switched off D or on E. Here, ϑ is the angle between the wall normal and the orientation of the rods: $\cos\vartheta=\hat{z}\cdot\hat{\omega}$ and $\Phi_0=10k_BT$. The Heaviside step function is defined by $\Theta(x)=1$ if $x\geq 0$ and 0 if $x<0$.

	Setups	$V_{\text{ext}}(\mathbf{r},\omega,t)$
A	Slow compression	$V_0\left(\frac{z}{Z(t)}\right)^{10}, \quad Z(t)=\begin{cases}2\sigma & \text{if } t<0,\\ 2\sigma-ct & \text{if } 0\leq t\leq\tau_B,\\ \sigma & \text{if } t>\tau_B\end{cases}$
B	Slow expansion	$V_0\left(\frac{z}{Z(t)}\right)^{10}, \quad Z(t)=\begin{cases}\sigma & \text{if } t<0,\\ \sigma+ct & \text{if } 0\leq t\leq\tau_B,\\ 2\sigma & \text{if } t>\tau_B\end{cases}$
C	Instantaneous expansion	$V_0\left(\frac{z}{Z(t)}\right)^{10}, \quad Z(t)=\begin{cases}\sigma & \text{if } t<0,\\ 2\sigma & \text{if } t\geq 0\end{cases}$
D	Relaxation from initial alignment	$V_0\left(\frac{z}{2\sigma}\right)^{10}-\Phi_0\cos^2\vartheta\Theta(-t)$
E	Evolution toward alignment	$V_0\left(\frac{z}{2\sigma}\right)^{10}-\Phi_0\cos^2\vartheta\Theta(t)$

time evolution of $\rho(z,\vartheta,t)$ to the new equilibrium state. Note that in the first scenario the external field primarily couples to the translational degree of freedom, whereas in the second one the orienting field acts only on the rod orientations. Both cases will provide insight into the intricate interplay between the translational and orientational degrees of freedom during the dynamic processes.

As a final input for the dynamics, we need to specify the diffusion constants $D_\perp$, $D_\parallel$, and D_r. For these, we take the results for hard ellipsoids of variable aspect ratio p reported by Tirado and co-workers [38]:

$$D_\perp=\frac{D_0}{4\pi}(\ln p+0.839+0.185/p+0.233/p^2),$$

$$D_\parallel=\frac{D_0}{2\pi}(\ln p-0.207+0.980/p-0.133/p^2),$$

$$D_r=\frac{3D_0}{\pi L^2}(\ln p-0.662+0.917/p-0.050/p^2), \qquad (23)$$

where D_0 sets the unit of time via $\tau_B=\sigma^2/D_0$. In all cases, the hydrodynamic aspect ratio of the rods was fixed at $p=5$. To justify the use of the mean-field functional, we fix the overall system number density to $\rho_0\sigma^3=1$, which is close to the overlap concentration of the rods.

Benchmark data to test our DDFT results were obtained by Brownian dynamics (BD) simulations of the segment model introduced in Sec. III. The simulation method is based on a standard finite-difference integration of the overdamped Langevin equations for N Brownian rods according to the scheme of Ermak [39,40]. We simulated $N=100$ rods each with $N_S=3$ segments in a slab geometry with periodic boundary conditions in the x and y directions. In all simulations, the time step was fixed at $0.001\tau_B$. Instantaneous density profiles were measured by averaging over 1000 consecutive dynamical processes each starting from a different initial equilibrium configuration. Each process was followed for the duration of about $15-20\tau_B$. To check for finite-size effects, additional simulations were carried out for $N=500$ rods yielding virtually identical results in all setups.

V. RESULTS

In this section, we present the results obtained by DDFT and Brownian dynamics simulation for the setups introduced in the preceding section. For each situation we show the time evolution of the density profile

$$\rho(z,t)=\int d(\cos\vartheta)\rho(z,\vartheta,t) \qquad (24)$$

and of the local nematic order parameter

$$S(z,t)=\frac{1}{\rho(z,t)}\int d(\cos\vartheta)\left[\frac{3}{2}\cos^2\vartheta-\frac{1}{2}\right]\rho(z,\vartheta,t) \qquad (25)$$

for a sequence of times. The nematic order parameter gives insight into the preferred direction of the rods. It is unity if the rods are perfectly oriented perpendicular to the wall and $S=-0.5$ if the rods are oriented parallel to the wall.

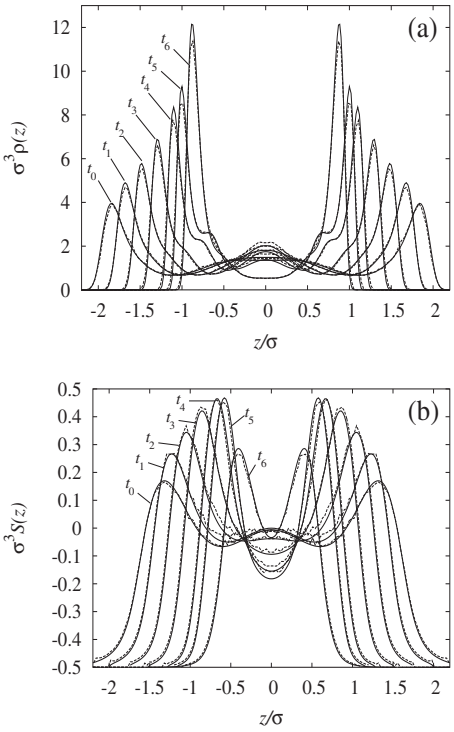

FIG. 3. DDFT (solid curves) and BD (dashed curves) results for (a) the time-dependent density profile $\rho(z,t)$ and (b) order parameter $S(z,t)$ for the slow compression; see A in Table I. The profiles correspond to the following time sequence: $t_0=0.0$, $t_1=0.2\tau_B$, $t_2=0.4\tau_B$, $t_3=0.6\tau_B$, $t_4=0.8\tau_B$, $t_5=0.9\tau_B$, and $t_6=15.0\tau_B$. At t_6 the system has virtually relaxed to equilibrium.

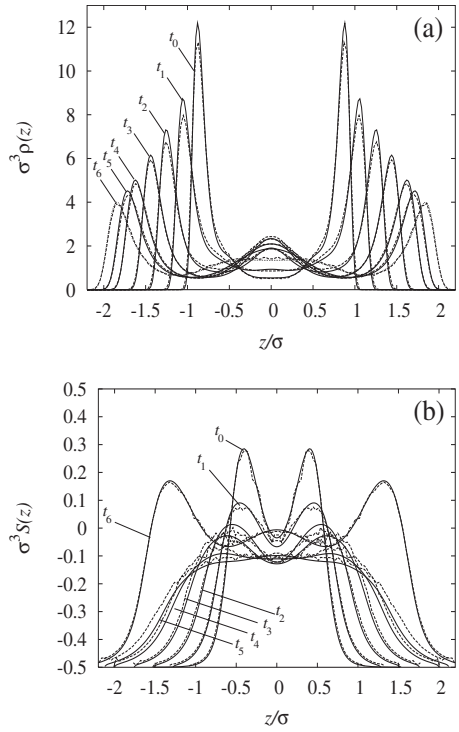

FIG. 4. DDFT (solid curves) and BD (dashed curves) results for (a) the time-dependent density profile and (b) order parameter for the inverse case to Fig. 3, the slow expansion; see B in Table I. The profiles correspond to the following time sequence: $t_0=0.0$, $t_1=0.2\tau_B$, $t_2=0.4\tau_B$, $t_3=0.6\tau_B$, $t_4=0.8\tau_B$, $t_5=0.9\tau_B$, and $t_6=15.0\tau_B$. At t_6 the system has virtually relaxed to equilibrium and the curves coincide with the initial ones, t_0, in Figs. 3(a) and 3(b).

A. Compression and expansion

First we examine the compression and expansion setups A, B, and C in Table I. The associated profiles are shown in Figs. 3–5. From all figures it can be seen that the theory correctly reproduces the time evolution of the density and nematic order parameter profiles. Looking first at the evolution of the nematic order parameter $S(z,t)$, we find a qualitative difference between the slow compression and expansion processes. Upon compression, the rods show enhanced *homeotropic* ordering (perpendicular to the wall), whereas the expansion process seems to be associated with pronounced *planar* ordering (parallel to the wall).

The first effect can be inferred from the overshoot in the nematic order parameter profile compared to the final equilibrium one; see Fig. 3(b). During the slow expansion, $S(z)$ gradually becomes negative indicating an orientational relaxation path characterized by the rods being preferentially oriented parallel to the wall [Fig. 4(b)].

This effect becomes even more pronounced for the instantaneous expansion, shown in Fig. 5(b). Here, the initially depleted area is flooded with rods that are strongly oriented parallel to the walls. This is best seen for the curves t_1, t_2, and t_3 in Fig. 5(b) where $S<-0.4$ close to the walls.

Both expansion processes B and C roughly consist of two steps. First, the initial two peak structure of $S(z,t)$ rapidly vanishes within the time interval of about 1 τ_B. Second, a slow evolution (spanning multiple τ_B) toward the final three peak structure is observed. On the contrary, for the slow compression case the initial two peak structure is preserved throughout the process and the weak third peak at $z=0$ slowly fades.

Now we turn our attention to the time evolution of the density profiles $\rho(z,t)$. For the slow compression, the preferred homeotropic alignment corresponds to a *shoulder* in the density profiles [see t_4 and t_5, Fig. 3(a)]. Note that it is not present in the final equilibrated configuration: t_6 in Fig. 3(a). Due to the increased local homeotropic alignment, there is an excess of rods with position $Z-L/2\geq|z|\geq Z$ which gives rise to the shoulder.

Apart from the shoulder, the density profiles for the slow expansion and compression processes seem very similar. Both show a layering effect that becomes manifest by a third peak emerging at $z=0$. This is most pronounced for $t\approx 0.5\tau_B$, where the effective wall-wall distance is such that three layers of rods can be accommodated between the walls. For the sudden expansion, the correlation peaks vanish completely during the relaxation process and the path toward the new equilibrium state goes via a four-peak structure illustrated by curve t_4. Another difference is that the planar oriented rods give rise to an overshoot in the correlation peaks compared to the final equilibrated profile; see t_5 and t_6.

In order to quantify the described asymmetry of the path of the different processes we calculate the second moment of the density, defined as

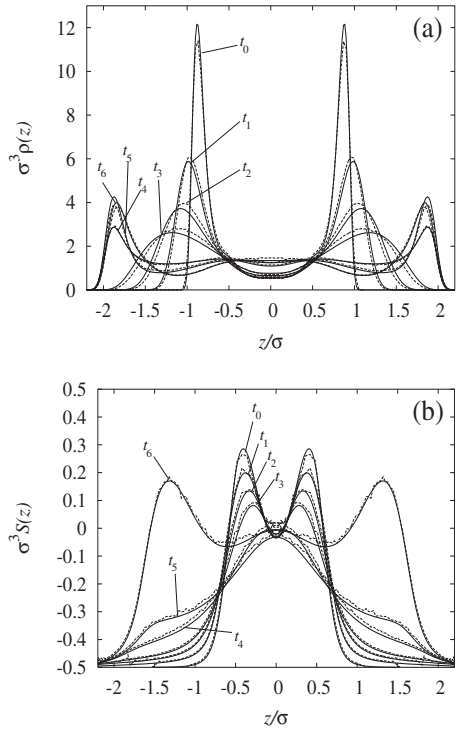

FIG. 5. DDFT (solid curves) and BD (dashed curves) results for (a) the time-dependent density profile and (b) order parameter for the instantaneous expansion; see C in Table I. The profiles correspond to the following time sequence: $t_0=0.0$, $t_1=0.02\tau_B$, $t_2=0.04\tau_B$, $t_3=0.06\tau_B$, $t_4=0.08\tau_B$, $t_5=0.25\tau_B$, and $t_6=15.0\tau_B$. The initial curves and those for t_6 coincide with the corresponding ones in Fig. 4.

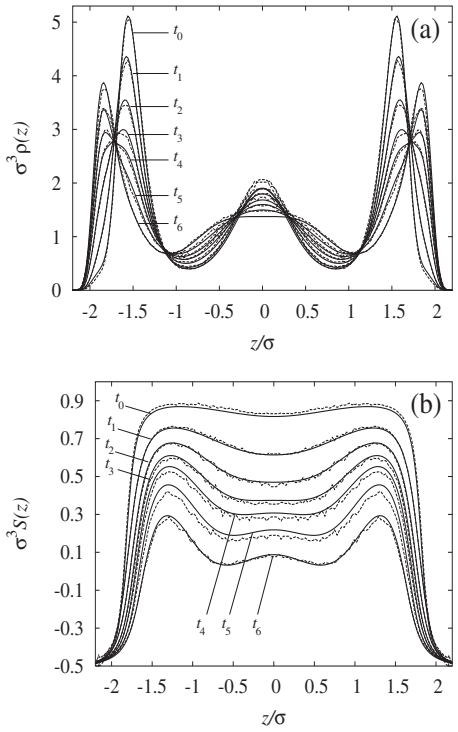

FIG. 7. DDFT (solid curves) and BD (dashed curves) results for (a) the time-dependent density profile and (b) order parameter for the relaxation of an initially aligned state; see D in Table I. The profiles correspond to the following time sequence: $t_0=0.0$, $t_1=1.0\tau_B$, $t_2=2.0\tau_B$, $t_3=3.0\tau_B$, $t_4=4.0\tau_B$, $t_5=6.0\tau_B$, and $t_6=15.0\tau_B$.

$$m_2(t) = \int dz\, z^2[\rho(z,t) - \rho(z,t=\infty)]. \tag{26}$$

The quantity $m_2(t)$ is a measure of the spread of $\rho(z,t)$ around its center. The resulting curves are shown in Fig. 6. In a similar study for spherical particles [29], it was found that

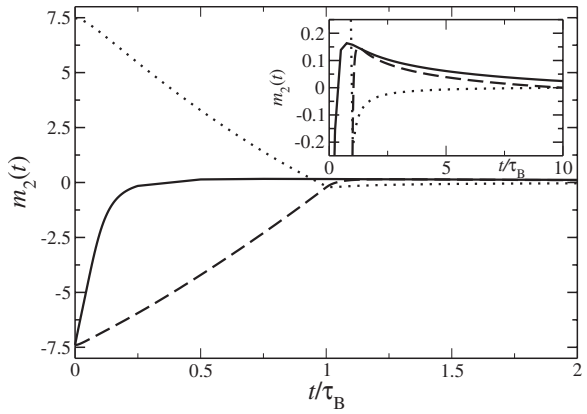

FIG. 6. Second moment of the density profiles, $m_2(t)$, versus time t. The full curve corresponds to the instantaneous relaxation C, the long-dashed curve to the continuous relaxation B, and the short-dashed curve to the compression A, respectively. The inset shows a magnified view of the same curves for small values of $m_2(t)$.

$m_2(t)$ behaves *monotonically* and can be best fitted to a single-exponential function for the expansion case and to a double-exponential function for the compression process. Here, $m_2(t)$ turns out to be a *nonmonotonic* function of time for all three processes which precludes a simple description in terms of an exponentially decaying function. From this we may already conclude that there is an interesting interplay between rotational and translational dynamics not found in systems of spherical particles.

The complicated relaxational behavior found here is related to the nonmonotonous evolution of the density profiles due to a transient enhanced localization of rods, viz. the shoulders emerging during the compression process. Finally, we note that in all three setups the reorientation process toward the new equilibrium state is approximately an order of magnitude slower than the initial relaxation of the positional degrees of freedom of the rods.

B. Orienting external field

We will now focus on the setups D and E in Table I, a slab confinement of fixed wall separation with an additional orienting field. We investigate both the relaxation from an initially aligned state by instantaneously switching off the field (Fig. 7) and the opposite case, in which a system is driven

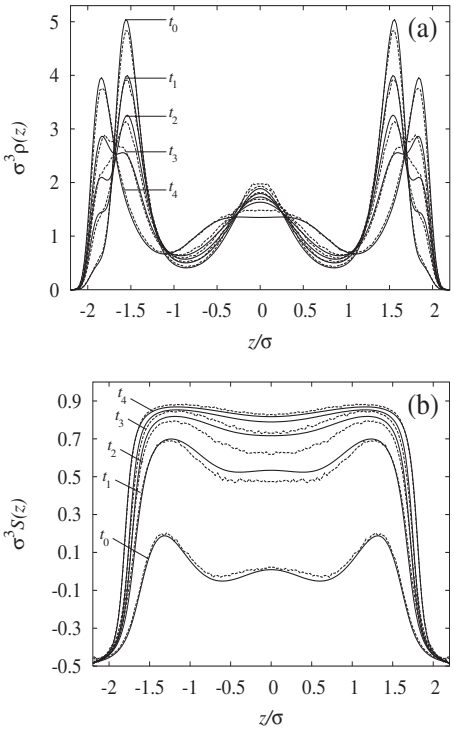

FIG. 8. DDFT (solid curves) and BD (dashed curves) results for (a) the time-dependent density profile and (b) order parameter for the inverse case to Fig. 7, the evolution toward an aligned state; see E in Table I. The profiles correspond to the following time sequence: $t_0=0.0$, $t_1=3.0\tau_B$, $t_2=5.0\tau_B$, $t_3=7.0\tau_B$, and $t_4=20.0\tau_B$.

into an aligned state after the field is switched on (Fig. 8). For the relaxation process both density and order parameter profiles agree very well with the simulation results. For the aligning process, however, larger discrepancies are found, especially in the nematic order parameter profiles. Here, the orienting process seems to be faster in the DDFT than in the BD simulations. (See Fig. 8(b).) A possible explanation is that the fast aligning process generates additional dynamic correlations that are not accounted for by the adiabatic assumption in our DDFT.

Although the external orienting field couples only to the orientation of the rods, the positions are also clearly affected. By forcing the rods to orient perpendicular to the wall, rod overlaps will be more common and the system will feel an effective compression. As a result, layering becomes more prominent, as we see from the sharpening of the density peaks in Fig. 8(a). The order parameter profiles show that the rods strongly orient perpendicular to the wall when the orienting field is switched on resulting in a value close to unity. Only very close to the walls do the rods lie parallel but the local density there is rather low.

In order to demonstrate the asymmetry of the two processes, we show the absolute values of the second moment in Fig. 9. First of all, the two data for $m_2(t)$ fall on different curves showing that the processes are asymmetric. Still both systems need approximately the same time to equilibrate, roughly $20\tau_B$. Furthermore, the log-linear plot shown in the inset shows that there are clear deviations from a straight line. Hence again the behavior is not a single exponential

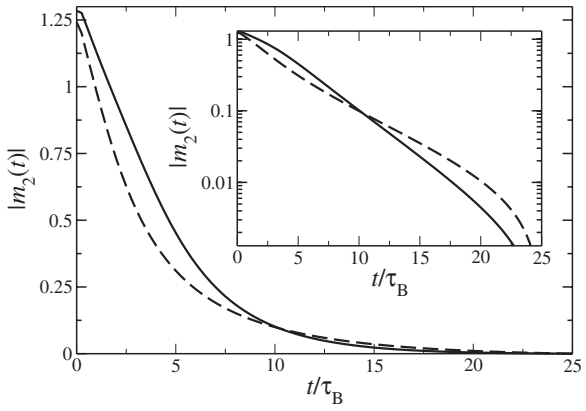

FIG. 9. Absolute value of the second moment $m_2(t)$ of the density profiles defined in Eq. (26) against time t. The full curve shows $|m_2(t)|$ for the situation when the orienting field is switched on E and the long-dashed curve the inverse D. The inset shows a logarithmic plot of the same.

function in time. In contrast to the compression and expansion the time evolution of $m_2(t)$ is a monotonous function of t for both situations.

VI. CONCLUSIONS

We have presented a formalism to predict the dynamical evolution under nonequilibrium conditions for anisotropic colloidal particles. The input needed for this theory is the equilibrium free energy density functional. Within a mean-field approximation for the functional valid for bounded Gaussian segment-segment interactions, the relaxation dynamics was studied for rods confined in a slab geometry. Slab expansion and compression was studied as well as turning on and off an aligning external field. Good agreement with Brownian dynamics computer simulations was found. The relaxation was a nontrivial interplay between rotational and translational dynamics. The system chose different paths of relaxation upon compression and expansion implying that the sequence of density fields is not inversion symmetric, even not with a suitably scaled time variable.

The present formalism can be applied to describe both different systems and setups. For example, hard rods or platelets can be treated by more sophisticated density functionals as, e.g., within the fundamental measurelike approximation [41–43] and Yukawa-segment models can be described by a mapping onto effective hard spherocylinders [44]. Other setups concern switching dynamics in different aligning fields which is the basic process in a liquid-crystalline optical device [45–47], sedimentation problems in rodlike suspensions [48–51], and orientational dynamics in rotating light fields [52–55]. Furthermore, it would be interesting to study the orientational glass transition within the DDFT approach in order to explore whether the orientational and translational dynamics get frozen-in at the same densities or not [23,56]. For future studies, it would be challenging to incorporate shear flow in the dynamical density functional theory formalism in which case macroscopic solvent

flow will couple strongly to the orientation of rodlike particles [57,58]. We acknowledge that serious modifications have to be carried out to our present DDFT formalism in order to correctly account for the distorted pair correlation function due to the shear [59–61]. Finally, we think that the present approach will be helpful to describe solvation dynamics [62,63], the orientational diffusion of supramolecular aggregates (like proteins) in solution, and the dynamics of stiff polymers [64].

ACKNOWLEDGMENTS

We acknowledge helpful discussions with J. K. G. Dhont, D. Cleaver, A. Archer, A. Perera, A. Esztermann, and C. N. Likos. This project is financially supported by the Deutsche Forschungsgemeinschaft (SFB TR6, project section D1), the Rektoratsstipendium of the Universität Düsseldorf, and the European network of excellence SOFTCOMP (Proposal No. 502235-2).

[1] J. Z. Wu, AIChE J. **52**, 1169 (2006).
[2] Y. Singh, Phys. Rep. **207**, 351 (1991).
[3] Y. Rosenfeld, Phys. Rev. Lett. **63**, 980 (1989).
[4] Y. Rosenfeld, M. Schmidt, H. Löwen, and P. Tarazona, Phys. Rev. E **55**, 4245 (1997).
[5] N. Grewe and W. Klein, J. Math. Phys. **18**, 1729 (1977); **18**, 1735 (1977).
[6] C. N. Likos, A. Lang, M. Watzlawek, and H. Löwen, Phys. Rev. E **63**, 031206 (2001).
[7] A. J. Archer, J. Phys.: Condens. Matter **17**, 1405 (2005).
[8] U. M. B. Marconi and P. Tarazona, J. Chem. Phys. **110**, 8032 (1999).
[9] U. M. B. Marconi and P. Tarazona, J. Phys.: Condens. Matter **12**, A413 (2000).
[10] A. J. Archer and R. Evans, J. Chem. Phys. **121**, 4246 (2004).
[11] F. Penna, J. Dzubiella, and P. Tarazona, Phys. Rev. E **68**, 061407 (2003).
[12] M. Rex, C. N. Likos, H. Löwen, and J. Dzubiella, Mol. Phys. **104**, 527 (2006).
[13] M. Rex, H. Löwen, and C. N. Likos, Phys. Rev. E **72**, 021404 (2005).
[14] Garnet Kin-Lic Chan and R. Finken, Phys. Rev. Lett. **94**, 183001 (2005).
[15] A. J. Archer, J. Phys.: Condens. Matter **18**, 5617 (2006).
[16] A. J. Archer and M. Rauscher, J. Phys. A **37**, 9325 (2004).
[17] J. K. G. Dhont and W. J. Briels, J. Chem. Phys. **118**, 1466 (2003).
[18] J. K. G. Dhont and W. J. Briels, Phys. Rev. E **72**, 031404 (2005).
[19] A. Lang, C. N. Likos, M. Watzlawek, and H. Löwen, J. Phys.: Condens. Matter **12**, 5087 (2000).
[20] C. N. Likos, M. Schmidt, H. Löwen, M. Ballauff, D. Pötschke, and P. Lindner, Macromolecules **34**, 2914 (2001).
[21] S. Lecommandoux, F. Checot, R. Borsali, M. Schappacher, A. Deffieux, A. Brulet, and J. Cotton, Macromolecules **35**, 8878 (2002).
[22] S. Jha, S. Dutta, and N. B. Bowden, Macromolecules **37**, 4365 (2004).
[23] T. Theenhaus, R. Schilling, A. Latz, and M. Letz, Phys. Rev. E **64**, 051505 (2001).
[24] J. K. G. Dhont, *An Introduction to Dynamics of Colloids* (Elsevier Science, Amsterdam, 1996).
[25] C. G. Gray and K. E. Gubbins, *Theory of Molecular Fluids* (Clarendon Press, Oxford, 1984).
[26] R. Evans, Adv. Phys. **28**, 143 (1979).
[27] K. E. Gubbins, Chem. Phys. Lett. **76**, 329 (1980).
[28] A. J. Archer, J. Phys.: Condens. Matter **17**, S3253 (2005).
[29] J. Dzubiella and C. N. Likos, J. Phys.: Condens. Matter **15**, L147 (2003).
[30] C. P. Royall, J. Dzubiella, M. Schmidt, and A. van Blaaderen, Phys. Rev. Lett. **98**, 188304 (2007).
[31] F. Penna and P. Tarazona, J. Chem. Phys. **119**, 1766 (2003).
[32] A. Poniewierski and R. Holyst, Phys. Rev. A **38**, 3721 (1988).
[33] L. Onsager, Ann. N.Y. Acad. Sci. **51**, 627 (1949).
[34] A. Chandra and B. Bagchi, Physica A **169**, 246 (1990).
[35] A. Chandra and B. Bagchi, J. Phys. Chem. **91**, 1829 (1989).
[36] H. H. Wensink (unpublished).
[37] A. Chrzanowska, P. I. C. Teixeira, H. Ehrentraut, and D. J. Cleaver, J. Phys.: Condens. Matter **13**, 4715 (2001).
[38] M. M. Tirado, C. L. Martinez, and J. G. de la Torre, J. Chem. Phys. **81**, 2047 (1984).
[39] D. L. Ermak, J. Chem. Phys. **62**, 4189 (1975).
[40] T. Kirchhoff, H. Löwen, and R. Klein, Phys. Rev. E **53**, 5011 (1996).
[41] D. de las Heras, E. Velasco, and L. Mederos, Phys. Rev. Lett. **94**, 017801 (2005).
[42] E. Velasco, L. Mederos, and D. E. Sullivan, Phys. Rev. E **62**, 3708 (2000).
[43] A. Esztermann, H. Reich, and M. Schmidt, Phys. Rev. E **73**, 011409 (2006).
[44] H. Graf and H. Löwen, Phys. Rev. E **57**, 5744 (1998).
[45] F. Barmes and D. J. Cleaver, Chem. Phys. Lett. **425**, 44 (2006).
[46] D. Marenduzzo, E. Orlandini, and J. M. Yeomans, Europhys. Lett. **71**, 604 (2005).
[47] D. Marenduzzo, E. Orlandini, and J. M. Yeomans, Mol. Cryst. Liq. Cryst. **401**, 171 (2003).
[48] A. P. Philipse, Curr. Opin. Colloid Interface Sci. **2**, 200 (1997).
[49] S. V. Savenko and M. Dijkstra, Phys. Rev. E **70**, 051401 (2004).
[50] F. M. van der Kooij, A. P. Philipse, and J. K. G. Dhont, Langmuir **16**, 5317 (2000).
[51] Z. Dogic, A. P. Philipse, S. Fraden, and J. K. G. Dhont, J. Chem. Phys. **113**, 8368 (2000).
[52] R. Kirchhoff and H. Löwen, J. Phys.: Condens. Matter **17**, 7805 (2005).
[53] R. Kirchhoff and H. Löwen, Europhys. Lett. **69**, 291 (2005).
[54] A. I. Bishop, T. A. Nieminen, N. R. Heckenberg, and H. Rubinsztein-Dunlop, Phys. Rev. A **68**, 033802 (2003).
[55] Z. Cheng, P. M. Chaikin, and T. G. Mason, Phys. Rev. Lett. **89**, 108303 (2002).
[56] M. Letz, R. Schilling, and A. Latz, Phys. Rev. E **62**, 5173 (2000).
[57] Y. G. Tao, W. K. den Otter, and W. J. Briels, Phys. Rev. Lett. **95**, 237802 (2005).
[58] Y. G. Tao, W. K. den Otter, J. K. G. Dhont, and W. J. Briels, J.

Chem. Phys. **124**, 134906 (2006).
[59] J. K. G. Dhont, Phys. Rev. Lett. **76**, 4269 (1996).
[60] U. Marini Bettolo Marconi and P. Tarazona, J. Chem. Phys. **124**, 164901 (2006).
[61] U. Marini Bettolo Marconi and S. Melchionna, J. Chem. Phys. **124**, 164901 (2006).
[62] B. Bagchi and A. Chandra, J. Phys. Chem. **97**, 5126 (1992).
[63] R. Ramirez and D. Borgis, J. Phys. Chem. **109**, 6754 (2005).
[64] M. Doi and S. F. Edwards, *The Theory of Polymer Dynamics*, 1st ed. (Clarendon Press, Oxford, 1986).
[65] Ellipsoidal Gaussian particles were recently studied in S. Prestipino and F. Saija, J. Chem. Phys. **126**, 194902 (2007).